Selective alkylation by zeolite catalysis opens up a sustainable platform of bisphenol substitutes from biomass.

Laura Trullemans
KU Leuven https://orcid.org/0000-0002-1945-0955
Steven-Friso Koelewijn
KU Leuven
Elias Cooreman
KU Leuven
Tessy Hendrickx
KU Leuven https://orcid.org/0000-0003-1564-5402
Gert Preegel
KU Leuven
Imke Boonen
Vrije Universiteit Brussel (VUB)
Joost Van Aelst
KU Leuven
Hilda Witters
Flemish Institute for Technological Research (VITO)
Marc Elskens
Vrije Universiteit Brussel (VUB)
Peter Van Puyvelde
KU Leuven https://orcid.org/0000-0001-7831-8682
Michiel Dusselier
KU Leuven
Bert Sels (bert.sels@kuleuven.be)
KU Leuven https://orcid.org/0000-0001-9657-1710

Article

Keywords:

Posted Date: April 6th, 2022

DOI: https://doi.org/10.21203/rs.3.rs-1505830/v1

Version of Record: A version of this preprint was published at Nature Sustainability on August 28th, 2023. See the published version at https://doi.org/10.1038/s41893-023-01201-w.

Abstract

Sustainable bisphenol A (BPA) substitutes should be safe and renewable to abolish the environmental burden of BPA's endocrine disruption and petrochemical origin. Suitable alternatives preferably also retain the rigid and stiff methylenediphenol (MDP) scaffold to emulate the hallmark performance of BPA-based polymers. Here, we report a holistic solution to sustainable BPA substitutes made from abundant lignin-derivable *o*-methoxyphenols that display low-to-undetectable xeno-estrogenic activity while preserving the MDP scaffold. More specifically, we propose an innovative zeolite-catalyzed synthesis towards the similar albeit safer methylenediguaiacol (MDG) scaffold via Brønsted acid-catalyzed alkylation of guaiacol with different *p*-alkenylguaiacols yielding various so-called bisguaiacols. Zeolite catalysis favors regioselectivity and prompts higher rate and chemoselectivity for entropic reasons thanks to active site pocket confinement. Exploiting the intrinsic handles present in *o*-methoxyphenols not only simplifies and ameliorates classic bisphenol chemistry, but also enables to design out xeno-estrogenic activity. Successful direct reaction of a crude lignin oil extract, as produced by reductive catalytic fractionation, highlights the feasibility and robustness of this route as a downstream process for future wood biorefineries. Last but not least, pure *p,p'*-bisguaiacols are polymerized into high-molecular weight thermoplastic and thermosetting polymers with promising thermo-physical properties. Overall, this work elucidates that renewability should not merely serve as a goal (renewable carbon), but also as a means (safer chemicals), thereby transcending the scope of renewability.

Introduction

Bisphenols, such as bisphenol A (BPA), are a unique class of diol polymer precursors that are pivotal for manufacturing plastics with superior thermal and mechanical properties.[1,2] The intrinsic rigidity and stiffness of the *p,p'*-methylenediphenol (MDP) scaffold is herein key.[3] These properties make bisphenols, and especially BPA, necessary for the polymer industry.[4]

Despite its indispensability, BPA is controversial. Its ability to interfere with natural estrogen receptors has long been known,[5] but came back into dispute when its leaching from polymers was found.[6–9] Ever since, BPA is scrutinized and linked to numerous adverse effects on human health and the environment.[10–15] These circumstances led to the quest for viable and harmless BPA alternatives.[16–20]

Even though a plethora of BPA replacements have been proposed, only few alternatives have been reported with significantly lower estrogenic activity.[21–26] One very promising strategy to design minimal estrogenic bisphenols involves incorporating *o*-methoxy moieties.[27–30] Interestingly, the natural design of the aromatic lignin biopolymer contains such a favorable substitution pattern in abundance.[31] Thanks to recent selective fractionation and depolymerization strategies of wood lignin, monomeric *o*-methoxyphenols become readily accessible as platform chemicals from several lignocellulosic biorefineries.[32–42]

Aside from the *o*-methoxy safety feature, high-yield and regioselective synthesis strategies that combine the *p,p'*-MDP scaffold with *o*-methoxy-substitution are scarce.[43,44] In common bisphenols, the bridging carbon is derived from a ketone or aldehyde that reacts twice with phenol *via* a two-step hydroxyalkylation-alkylation condensation (Fig. 1a). Existing methods to the *o*-methoxy-substituted *p,p'*-MDP scaffold – a so-called *p,p'*-methylenediguaiacol (MDG) scaffold or bisguaiacol, may follow an identical mechanism (e.g. for bisguaiacol A),[43] or use an improved one-step electrophilic alkylation condensation (e.g. for bisguaiacol F), which avoids the hydroxyalkylation step.[45] The former approach requires volatile organic alkylation agents, *viz*. acetone as coupling agent, homogeneous or thermo-labile catalysts, and sulphur-containing co-catalysis to promote *p,p'*-regioselectivity and enhance the reaction rate, whereas the latter synthesis route is prone to substantial loss of material due to oligomerization (up to 30 wt.%).[45,46] Moreover, both methods release stoichiometric amounts of condensation water that impede the chemical kinetics, catalyst activity, and reaction homogeneity.[47–49]

In this work, we propose an innovative route towards *p,p*'-bisguaiacols starting from renewable *o*-methoxyphenol (guaiacol) and various *p*-alkenylmethoxyphenols. Our strategy relies on Brønsted acid-catalyzed Friedel-Crafts alkylation chemistry between an arene and alkene molecules (Fig. 1b). Alkenes, such as *p*-propenylguaiacol (isoeugenol) and *p*-propenylsyringol,[50,51] as well as the corresponding *o*-methoxyphenols,[39] have recently been identified as major products obtained from (wood) lignin fractionation and depolymerization. Interestingly, using such bio-aromatic alkenes for carbon-carbon coupling avoids the release of condensation water, and hence allows to explore the advantages of (otherwise water-sensitive) zeolites. Zeolites are microporous crystalline solids that are widely used as safe, stable, and strong Brønsted acid catalysts in the industry (e.g. oil refining).[52] It appears that the unique spatial organization of the (Brønsted acid) active sites in the molecular-sized pores can have a marked beneficial effect on product selectivity.[49]

Our proposed zeolite-catalyzed alkylation strategy can selectively provide good-to-excellent yields of renewable and safer bisphenol substitutes. Hereto, a family of bisguaiacols is made from various commercially available *p*-alkenylguaiacols (Fig. 1b). The potential growth of the proposed platform by further extension of the substrate scope is shown in Supplementary Figure S1. The synthesis method, developed with pure compounds, is experimentally validated by using a real lignin-derived bio-aromatic alkene, thus demonstrating the first step feasibility of this bio-route. Sustainability of the synthesis benefits from the use of strong but harmless zeolite acidity and its recyclability. The *in vitro* estrogenic activity of the novel bisguaiacols, tested here via two different bioassays, is *a priori* evaluated to avoid any regrettable substitutions in polymers later. Finally, the technical functionality of the safer and renewable bisguaiacols is confirmed in polymer chemistry, *viz*. synthesis of thermoplastics (i.e. polycarbonates and polyesters) and a thermoset (i.e. epoxy resin).

Results

Concept validation. The commercially available *o*-methoxyphenols guaiacol (G) and isoeugenol (IE, **1a**) were selected to validate the proposed Friedel-Crafts alkylation concept. The general reaction pathway to alkylate G with aromatic alkenes (**1a-e**) with acidic protons is shown in Fig. 2a. Before testing acidic zeolites, the alkylation was verified by soluble acids such as common mineral acids, sulfonic acids and (hetero)polyacids (Supplementary Fig. S2a-c). Reactions were done in an excess of G to obviate auxiliary solvent usage.

The two major product classes (Fig. 2a; Supplementary Fig. S3) detected by gas and liquid chromatography analyses (i.e. GC-FID and HPLC-UV) (Supplementary Fig. S4a-b) and (retroactively) identified by mass spectrometry (i.e. GC-MS) and 1D,2D nuclear magnetic resonance (NMR) analyses were so-called bisguaiacols (**2a**) and cyclic dimers (**3a**). The class of **2a** consists of three regioisomers (*o,p'-*, *m,p'-* and *p,p'-***2a**) since alkylation of G by **1a** can occur in *ortho*, *meta* or *para* position (relative to the hydroxyl) (Supplementary Fig S5-7). The class of **3a** consists of two diastereoisomers (α- and γ-**3a**) arising from self-dimerization of **1a** by acid-catalyzed cycloaddition (Supplementary Fig. S8-9). Conversions and theoretical product yields are calculated in mol% based on the initial alkene content. The chemo- and regioselectivity (in mol%) are defined as the product selectivity of **2a** to the sum of **2a** and **3a** and *p,p'-***2a** to all isomers, respectively. More details are provided in the caption of Fig. 2 and Supplementary Methods 3.

In batch (B) reaction set-up, out of all soluble acids tested, sulfuric acid (H_2SO_4) performed best (Supplementary Fig. S2a-c). H_2SO_4 gave high conversion (98%) but low chemoselectivity (38%) yielding 61% of **3a** and only 19% of **2a** (77% *p,p'-*, 16% *m,p'-* and 7% *o,p'-***2a**) (Fig. 2b). Moreover, gel permeation chromatography analysis (i.e. GPC-PDA) showed the presence of higher molecular weight (MW) compounds, likely due to cationic self-oligomerization of **1a**, explaining the 18% carbon balance deficit (Supplementary Fig. S4c).

Prompted by the seemingly higher reaction order in **1a** for self-dimerization (to **3a**) compared to alkylation (to **2a**), the reactor set-up was changed into fed-batch (FB) – gradually feeding pure **1a** into G – to enhance chemoselectivity. In doing so, the product distribution almost inverted, tripling the yield of **2a** to 61% of **2a** with only 28% of **3a**, thereby raising the chemoselectivity to 81% (Fig. 2b). No change in regioselectivity was observed upon switching from B to FB set-up.

Chemo- and regioselective heterogeneous zeolite catalysis. The sustainable production of chemicals implies the use of robust and recyclable heterogeneous catalysis. Whereas solid sulfonic acids are promising alternatives to soluble acids, zeolites, which are used today in petrochemistry, are famous for their confinement effects, also called shape-selectivity in zeolite jargon, guiding a reaction towards, sometimes unexpected, product selectivity advantages.[49,52] The intuitively lower steric constraints of the reaction to form bisguaiacols (**2a**) relative to those for cyclic dimers (**3a**) encouraged us to study the effect of active site confinement on the chemoselectivity (as well as the regioselectivity).

Over 20 heterogeneous non-zeolite and zeolite catalysts were evaluated in B conditions (Supplementary Fig. S2d-e) out of which four catalysts (viz. Amb-15, H-ZSM-5, H-USY, H-BEA) were selected and screened in FB mode (Fig. 2b, left; Supplementary Fig. S10). Plotting chemoselectivity against yield (Fig. 2b, right) reveals that only the 12-membered ring zeolite H-USY performed better than H_2SO_4. H-USY was highly active and chemoselective (90%) yielding 75% of **2a** and only 16% of **3a** at full conversion while also showing better regioselectivity (82% *p,p'*-, 15% *m,p'*- and 3% *o,p'*-**2a**). In contrast, Amberlyst 15 – a polymeric proton-exchange resin commercially applied in industrial BPA production – showed incomplete conversion (86%) and favored undesirable **3a** formation under otherwise **2a**-favoring FB conditions. These results accentuate the zeolite's potential to delicately control product selectivity upon alkylation of G with **1a**. That not every zeolite is equally successful is related to differences in acid strength, acid site accessibility and acid site spatial confinement. For instance, the 12-membered ring zeolite H-Beta, another member of the large pore zeolite family, also reached full conversion, but showed considerably lower chemoselectivity (73%), yielding only 53% of **2a** with a lower regioselectivity (71% *p,p'*-, 23% *m,p'*- and 6% *o,p'*-**2a**) as compared to H-USY (and H_2SO_4). The 10-membered ring zeolite H-ZSM-5 was least active, reaching 56% conversion, giving very low yields of **2a**, even in FB mode. The low conversion is consistent with the inability of large reagents (such as **1a**) to reach the active sites inside the small pores of the zeolite crystals.

Besides the ability to tune product selectivity, zeolites are also known for their high thermal stability, in contrast to, for example, Amberlyst 15. This enables thermal catalyst rejuvenation, a prerequisite to establish a sustainable catalytic process. Looking into the recyclability of the H-USY zeolite, it was found that the activity of the spent zeolite was completely restored by calcination in air (Supplementary Fig. S11).

Entropic control of chemoselectivity. The improved chemoselectivity at low concentrations of **1a** achieved either via pseudo-high dilution in FB mode or high dilution in B mode (Supplementary Fig. S12) may suggest that physical barriers rather than chemical (kinetic) reasons are at the basis of the even higher chemoselectivity seen for H-USY. Thereto first the mass diffusion explanation was investigated (and excluded) by performing a detailed kinetic study. The procedures for the kinetic analysis are described in full in Supplementary Methods 4. Figure 3a illustrates the kinetic profile for both the (confined) H-USY and the (unconfined) H_2SO_4 catalytic system at 80 ^oC (under equimolar proton conditions) with rates defined in turn-over frequency (TOF) for *p,p'*-**2a** and α-**3a** formation. The plot clearly shows a three-fold higher TOF for **2a** in presence of H-USY, while **3a** formation runs equally fast. Temperature effects on the kinetics were determined, giving access to reaction orders (Supplementary Fig. S13-14, Table S1) and reaction activation energies (via Arrhenius Law) (Supplementary Fig. S15). Given the similar observed orders (n_{obs}) in **1a** for formation of **2a** and **3a**, respectively, *viz.* n_{obs} (**1a** to **2a**) ≈ 1 and n_{obs} (**1a** to **3a**) ≈ 2, for the two catalysts, invoking mass transport barriers (in the pores) to explain the high chemoselectivity in presence of H-USY seems unlikely. Catalysis under diffusion limitation free regime with H-USY is further supported by the significantly higher observed activation energies (E_a) for H-USY, being similarly

high for **2a** and **3a** formation (87.7 and 88.5 kJ mol^{-1}, respectively), compared to the lower values for H_2SO_4 (43.7 and 36.5 kJ mol^{-1}, respectively), suggesting a lower energy pathway for **3a**.

Additional Eyring-Polanyi analyses of the thermal reaction rate dependency provides access to the standard entropy $(\Delta S^{\ddagger})$ and standard enthalpy $(\Delta H^{\ddagger})$ of activation at the level of the transition state. (Fig. 3b, Supplementary Fig. S16, Table S2). The similarity of $\Delta H^{\ddagger}$ and E_a suggests that, irrespective of the catalyst, the reaction mechanism of both reactions (**1a** to **2a** and **1a** to **3a**) includes one (dominant) transition state. $\Delta S^{\ddagger}$ represents the change in entropy from the reactants initial state to the transition state. For H_2SO_4, $\Delta S^{\ddagger}$ values for **2a** and **3a** of -230.2 and − 212.1 J mol^{-1} K^{-1}, respectively, were found. Entropic changes towards transition-state formation were significantly lower for H-USY, showing a $\Delta S^{\ddagger}$ of -101.9 and − 66.7 J mol^{-1} K^{-1} for **2a** and **3a**, respectively. This suggests that the pores of H-USY create (along the reaction coordinate) molecular orientations that favor **2a** formation. Such pre-organization in the catalytic pocket, to favor reaction rate control and selectivity, is known in enzyme catalysis and recognized in nanoconfined catalysis.[53,54] Following the Gibbs free energy definition, $\Delta G^{\ddagger} = \Delta H^{\ddagger} - T\Delta S^{\ddagger}$, a lower change in entropy results in a lower Gibbs free energy of activation $\Delta G^{\ddagger}$. Hence, H-USY entropically favors formation of both **2a** and **3a** compared to H_2SO_4, but clearly with larger preference to form **2a** within the temperature window of reaction for H-USY (Fig. 3c).

Substrate scope expansion. Nature's intrinsic biodiversity provides a wide variety of plant-based *o*-methoxyphenols (Supplementary Fig. S17) that allow to expand the substrate scope and build a broader platform of bisphenol replacements. The applicability of our proposed zeolite-based process – preferably in FB mode – to other *p*-alkenylguaiacols such as 4-vinylguaiacol (**1b**), ferulic acid (**1c**), methyl ferulate (**1d**) and ethyl ferulate (**1e**) is encouraging (Fig. 2c).

The substrate's reactivity was screened both in B and, if liquid at RT, in FB set-up with H_2SO_4 and H-USY as catalysts (Fig. 2c). The products were identified by GC-MS and analyzed by GC-FID and GPC (Supplementary Figs. S18-19), after purification of the *p,p'*-isomer (2a-d) the molecular structure was confirmed by ^{1}H and ^{13}C, 1D- and 2D-NMR analysis (Supplementary Fig. S20-S22) and the bisguaiacols were retroactively quantified by GC-FID calibration.

In all cases, zeolite H-USY outperformed H_2SO_4, confirming its need for high yields of bisguaiacols (**2**). Noticeably, H-USY showed excellent chemo- (> 99%) and high regioselectivity (> 82%) toward **2c-e**. In this regard, it is worth mentioning that the water-free synthesis conditions withhold ester hydrolysis enabling a larger set of variations within the platform. Near full conversion of (≥ 95%) in presence of H-USY yields 93% of **2c** (with 83% *p,p'*-, 12% *m,p'*-, 4% *o,p'*-**2c** and < 1% others) and > 99% of **2d** (with 88% *p,p'*-, 7% *m,p'*-, 5% *o,p'*-**2d**) and 98% of **2e** (with 82% *p,p'*-, 11% *m,p'*-, 4% *o,p'*-2e and < 3% others). Reaction with **1b** (in FB) also shows full conversion with H-USY zeolite, yielding 51% of **2b** (with 84% *p,p'*-,12% *m,p'*- and 4% *o,p'*-**2b**) with a moderately high chemoselectivity of 78% (Fig. 2c). Despite being less selective, separation of this *p,p'*-bisguaiacol product from the crude appears surprisingly easy thanks to its spontaneous

crystallization. Oligomers, accounting for 19% yield, were identified as high MW polyvinylguaiacol (Supplementary Fig. S23-24), formed by cationic polymerization of **1b**.

To further strengthen the proposed zeolite-catalyzed alkylation strategy for bisguaiacols synthesis, we here show a comparison to the classic synthesis method. For the synthesis of **2a**, we were left with a less successful result using the reaction between G and propanal in the presence of H_2SO_4 and the thiol promotor (B, 100°C, 20 h). As reported in Fig. 2c left, low **2a** yield (55%) and unfavorable regioselectivity (58% *p,p'*-, 22% *m,p'*- and 15% *o,p'*-**2b** and 5% others) were obtained.

The *p,p'*-bisguaiacols of **2a**, **2b** and **2d** were synthesized on a multi-gram scale (e.g., up to 45 mmol, 13 g for **2a**) and purified (> 99.5%) by cooling crystallization from heptane. Preparative HPLC fractionation was used to isolate *p,p'*-**2c** given its sluggish crystallization. The color of **2a-d** varied from white to off-white (Fig. 5a). The thermal properties (T_m, T_d), as determined by dynamic scanning calorimetry (DSC) and thermogravimetric analysis (TGA), are reported in Fig. 5b-c, Supplementary Figure S25 and Table S3. Detailed comparison of the melting and stability properties of bisphenols and bisguaiacols, with or without *o*-methoxy moieties, such as BPE **(4c**) - BGE (**2b**) and BPF (**4b**) - BGF (**4e**) shows that the presence of the *o*-methoxy groups lowers T_m with 17°C and 57°C, respectively and $T_{d,max}$ with 44°C and 15°C, respectively. The significantly higher thermal stability ($T_{d,max} \geq 264$°C) of the two bisguaiacols **2c-d** indicates a beneficial role of the polar functional group on the carbon bridge. In general, the *p,p'*-bisguaiacol platform expands the physical properties, and therefore application potential (e.g. thermal window), with regard to the current state of the art, reaching or surpassing the properties of industrial bisphenols.

Early screening of xeno-estrogenic activity by in vitro **bioassays.** To avoid regrettable bisphenol replacements, the potential xeno-estrogenic activity of pure *p,p'*-**2a-d** relative to *p,p'*-**4e** (reference bisguaiacol) and *p,p*-**4a-c** (reference bisphenols) were *a priori* determined. Hereto, the *in vitro* transactivation of the human estrogen receptor α (hERα) was studied by two luciferase reporter gene assays using transgenic human MELN cells (MELN assay) and transgenic human VM7Luc4E2 cells (CALUX assay), benchmarked against the natural hormone 17β-estradiol (E2). The data is visualized in two ways (Fig. 4). While Fig. 4a shows the *in vitro* estrogenic transactivation against concentration (up to 10^{-3} M), Fig. 4b provides a scatter plot of (log-transformed) potency (i.e. concentration needed for a given effect, expressed as half-maximal effective concentration, EC_{50}) and efficacy (i.e. maximum effect induced for a compound relative to E2, expressed as relative estrogenic efficacy, REE). Hence, compounds with the lowest potency and efficacy our found in the bottom right corner. More details are provided in Supplementary Tables S4-6.

In both bioassays, as indicated by the concentration-response curves in Fig. 4a, the bisguaiacols are significant less potent (EC_{50} = 20–100 μM) and efficacious (REE's ≤ 68%) and hence possess less estrogenic activity than the common bisphenols (REE = 92–194%; EC_{50} = 0.1–5 μM) over the whole range tested (up to 10^{-3} M). It is worth mentioning that no EC_{50} values could be calculated (i.e. upper plateau

was not reached) for some bisguaiacols. This applied to **2c** in the MELN assay, and to **2c**, -**2d** and – **4e** in the CALUX assay.

Two independent one-way ANOVAs were conducted to compare the $\log_{10}(EC_{50})$ and REE values of both bioassays. F- and P-values are provided in Supplementary Table S7. For both assays, Tukey's HSD post-hoc analysis (Supplementary Table S8-11) indicated that all mean $\log(EC_{50})$ and REE pairs of the bisphenols and bisguaiacols were significantly different. For the MELN assay, mean $\log(EC_{50})$ differences ($\Delta\log(EC_{50})$) from – 0.8 up to -1.9, and REE mean differences (ΔREE) from 35% up to 183% were found. For the CALUX assay, $\Delta\log(EC_{50})$ values from – 1.3 up to -2.0 and ΔREE values from 71% up to 116% were reached. These statistical analyses point out that, based on both assays, all tested bisguaiacols are safer (in terms of *in vitro* estrogenic activity) than common industrial bisphenols. As previously reported[28,29], this study reconfirms that, by comparing to structural analogues (Supplementary Fig. S26, Tables S8-11), the *o*-methoxy groups significantly lowered the potency ($\Delta\log_{10}(EC_{50})$ = -1.1 up to -1.4) and efficacy (ΔREE from 76% up to 125%).

In addition, the Tukey's HSD post-hoc analysis provided more insight for safer bisguaiacol design. In terms of potency, both assays showed no discrepancy between **2a** and **2b**. In terms of efficacy, only **2c** was found significantly different from all other bisguaiacols in the MELN assay, while the CALUX assay didn't show any discrepancy (i) between **2c** (3.5%), **2d** (7.7%) and **4e** (6.2%), and (ii) between **2a** (20.5%) and **2b** (16.0%), dividing them in two significant different groups. Based on these results, the low, undetectable, estrogenic activity of **2c** seems to be induced by the polarity on the carbon bridge (**2a** vs. **2c**) rather than molecular size extension (**2a** vs. **2d**).

Because of their low agonist activities, the bisguaiacols' antagonist activity was screened as well to provide a comprehensive evaluation of the *in vitro* estrogenic activity. As shown in Supplementary Fig. S27 the bisguaiacols didn't show any inhibitory activity, since no decrease in activity could be detected over the whole concentration range when tested together with the EC_{50} of the reference standard (E2). Overall, the newly proposed *p,p'*-bisguaiacols can be considered as non-regrettable bisphenol alternatives based on our two *in vitro* estrogenic activity bioassays, both in agonistic and antagonist mode.

From plant to product. In what follows, an experimental proof of concept is presented to assess the potential of the above alkylation chemistry as a downstream process in future lignocellulosic biorefineries. Whereas *o*-methoxyphenols (e.g. G) are among the main products in many biorefinery schemes,[35,38,39] producing bio-aromatic alkenes is more difficult. Therefore, we aimed to produce a lignin oil rich in **1a** by tweaking the reductive catalytic fractionation (RCF) process; an emerging so-called 'lignin-first' biorefinery.[37,55] RCF combines lignin isolation/depolymerization to produce both a lignin oil rich in *o*-methoxyphenolics and a solid carbohydrate pulp, suitable for further valorization. Even though such *p*-alkenylphenols (e.g. coniferyl alcohol and **1a**) exist as reactive intermediates during RCF, they are sensitive to repolymerization into polyphenolics. Yet, here, a lignin oil (10 wt.% of monomers and 90 wt.% of oligomers) rich in **1a** (8 wt.% on total oil basis and 84 wt.% on total monomer basis) was successfully

produced by performing RCF on pine softwood (viz. 25 wt.% of lignin, 7 wt.% of hemicellulose, 63 of wt.% cellulose and 5 wt.% others) in biphasic solvent (water-butanol) under mild conditions (*viz.* low contact time, H_2 pressure and temperature). Further enrichment of the monomeric fraction via simple and efficient two-step liquid-liquid extraction yielded a lignin oil extract (51 wt.% of monomers and 49 wt.% of oligomers) enriched in **1a** (44 wt.% on total extract basis and 86 wt.% on total monomer basis) (Fig. 2d and Supplementary Fig. S28-29). The other 7 wt.% of monomers consists of *p*-methylguaiacol and *p*-propylguaiacol.

Next, the crude **1a**-rich extract was reacted with G in high dilution B mode. Under zeolite H-USY catalysis, this **1a** was fully converted (> 99%) yielding 76% of **2a** (80% *p,p'*-, 16% *m,p'*-, 4% *o,p'*-**2a**) with high chemoselectivity (91%) (Fig. 2d). Surprisingly, despite being less pure and more complex in composition, the crude extract gave results similar to reacting commercially available pure **1a** in FB operation (Fig. 2b). Other mono- and oligomeric compounds present in the crude extract hence do not seem to impede the zeolite-catalyzed alkylation, highlighting the robustness of the process.

Moreover, the product distribution of the crude extract after alkylation (Supplementary Fig. S29) shifted toward mainly dimers (61 wt.%) next to oligomers (35 wt.%) and monomers (4 wt.%). On product basis, dimers consist of 52 wt.% of **2a**, 6 wt.% of **3a** and only 3 wt.% of other lignin dimers (Fig. 2d). Based on the purification of *p,p'*-**2b** (*vide supra*), the isolation of **2a** via crystallization from this product mixture seems convenient for larger-scale productions. Hence, the downstream **2a** process following RCF would include: monomer extraction, alkylation reaction, distillation and crystallization in the future bioeconomy.

Towards high- T_g **aromatic polymers.** Encouraged by their significantly lower *in vitro* estrogenic activity and their renewability, ultimately, the bisguaiacols were assessed for their potential in polymer chemistry. Two thermoplastics, i.e. poly(*p,p'*-**2a**-terephthalate) (**2a**-PT) and poly(*p,p'*-**2a**-carbonate) (**2a**-PC) and one thermosetting resin, i.e. poly(*p,p'*-**2a**-epoxide) (**2a**-ER), cured with isophorone diamine (IPDA), were made together with BPA (**4a**)-based benchmarks. More details about the polymerization procedures are described in the Methods section.

Based on ^{1}H- and ^{13}C-NMR analyses (Supplementary Fig. S30-S32), the reactivity of *p,p'*-**2a** toward PT, PC and ER was confirmed, providing polymers in excellent yields (94–96%), which were castable/curable into transparent films/pucks (Fig. 5d-f). Key polymer characteristics are summarized in Fig. 5g. Noteworthy, *m,p'*- **4e** has been shown as reactive and functional as the *p,p'*- **4e**[29], implying that, although not examined here, mixtures of both **2a** isomers might be used as well.

For the thermoplastics, the mass-average molecular weight ($\overline{M}_w$) and dispersity (Đ) were estimated by size exclusion chromatography (SEC) analysis in THF (Supplementary S33-34a), indicating $\overline{M}_w$ = 132 kg mol^{-1} with Đ = 4.1 for **2a**-PT and $\overline{M}_w$ = 62 kg mol^{-1} with Đ = 7.3 for **2a**-PC (Fig. 4b). While reaching similar dispersity, the **2a**-based thermoplastics showed significantly higher $\overline{M}_w$ than the benchmarks (21 and 25 kg mol^{-1} for **4a**-PT and **4a**-PC, respectively). This remarkable difference in $\overline{M}_w$ is likely caused

by solubility differences since **2a**-PC was observed to be more soluble in the reaction solvent (DCM) than **4a**-PC. Since **4e**-PC was previously reported less soluble in DCM,[29] the higher solubility can be attributed to the propylidene bridge (and not the *o*-methoxy groups). The GPC/SEC chromatograms of **2a**-PC, and the benchmark **4a**-PC, showed the presence of compounds with a MW < 580 g mol^{-1}. Because of this low MW, the signals are rather assigned to substrates (i.e. incomplete conversion) than to macrocyclization reactions.[23,56]

The thermoplastics' thermal properties, i.e., glass-transition (T_g) and maximal weight loss temperature ($T_{d,max}$), were assessed by DSC and TGA under N_2, respectively (Fig. 5b and Supplementary Figs S33-34b,c). T_g and $T_{d,max}$ of the synthesized **4a**-PC are 118°C and 521°C, respectively, this T_g is 27°C lower than the T_g reported for a commercial **4a**-PC with similar $\overline{M}_w$ but Đ of 1.8.[57] Ideally Đ should be around 2.0, indicating that rather suboptimal reaction conditions were used.[58] Nevertheless, as both synthesized polycarbonates show similar Đ, the potential of **2a**-PC can be evaluated in comparison to **4a**-PC. **2a**-PC showed T_g of 101°C and $T_{d,max}$ of 444°C, being 15°C and 77°C lower, respectively, than the **4a**-PC benchmark. Although it has been shown that the presence of *o*-methoxy moieties lowers the polycarbonate's T_g and their thermal stability, it is fair to assume that, just like for **4a**-PC, the T_g of **2a**-PC with Đ ≈ 2.0 will be higher than 101°C, surpassing the thermal properties of the current state-of-the-art **4e**-PC with T_g of 106°C and $T_{d,max}$ of 418°C ($\overline{M}_w$ = 23 kg mol^{-1}, Đ = 3.8).[29]

2a-PT exhibits a T_g and $T_{d,max}$ of 166 and 425°C, respectively. Although lower than the benchmark **4a** polymer (Fig. 5d), **2a**-PT shows thermal properties close to the commercial high-performance BPA-PC references showing T_g around 145°C and $T_{d,max}$ around 500°C.[57,59,60] Moreover, a lower T_g (< 200°C) and better solubility in common solvents improves polymer processability, highlighting the potential applicability of **2a**-PT.[61,62]

For the thermosetting resins, the diglycidyl ether of **2a** (**2a**-DGE) was obtained as an off-white solid which melted at a substantially higher temperature (T_m = 94 °C) than the benchmark **4a**-DGE (T_m = 46 °C), i.e., BPA diglycidyl ether. However, **2a**-DGE remained as a metastable undercooled viscous liquid at RT once melted, which facilitates mixing with curing agents. When fully cured, **2a**-ER and **4a**-ER showed high degrees of curing (93%) and comparable thermal stability (DSC/TGA, Supplementary Fig. 35a-c, under N_2). Based on dynamic mechanical analysis (DMA) (Supplementary Fig. 35d), the T_g of **2a**-ER (117°C) was found to be markedly lower than of **4a**-ER (173°C), but still high enough to serve as a safer, renewable and functional alternative to BPA-based epoxy resins in various applications.

Discussion

Brønsted acid-catalyzed Friedel-Crafts alkylation between plant-based *o*-methoxyphenols, *viz.* arenes (e.g. guaiacol) and aromatic alkenes (e.g. isoeugenol) was envisaged as a viable chemistry towards sustainable BPA substitutes. However, for this chemistry to be chemoselective in the face of two

competitive reaction pathways, kinetic control had to be gained. This was achieved by keeping the alkene concentration at a minimum by either working in high dilution batch mode or in pseudo-high dilution fed-batch mode. Surprisingly, when using zeolite H-USY, shape-selective active site confinement also exerted entropic control over the transition-state, thereby enhancing both chemo- and regioselectivity. Taken together, chemo- and regioselective alkylation by zeolite catalysis (preferably) in pseudo-high dilution fed-batch mode granted access to multiple *p,p'*-bisguaiacols made from various guaiacol-based substrates. Closely related substrates, such as catechol (1,2-dihydroxybenzene), syringol (2,6-dimethoxyphenol) and 4-alkenyl-substituted derivatives thereof, might further extent the substrate scope, emphasizing the concepts' platform potential.

When extending the substrate scope, thereby creating potentially viable BPA replacements, the xeno-estrogenic activity should be carefully monitored already in the early design stage. For all newly proposed *p,p'*-bisguaiacols, the *in vitro* estrogenic activity was found to be significantly lower than for common bisphenols, or undetectable, even at concentrations up to 10^{-3} M, which is encouraging. Structure-activity relationships pointed at (and confirmed) the beneficial effect of incorporating *o*-methoxy groups as well as polarity on the bridging carbon. Nevertheless, to design out endocrine disruption of the next generation of chemicals, additional *in vitro* and *in vivo* bioassays need to be performed to exclude other adverse outcomes (e.g. (anti-)androgenicity, (anti-)thyroidicity, metabolic activation). In addition, the adequacy of bisguaiacol P for polyester, polycarbonate and epoxy resin synthesis was shown, resulting in high-T_g and thermal stable polymers, hence, demonstrating the potential of this safer, drop-in BPA substitute.

Even more so than the current state of the art, our alkylation process and products were designed to comply with the principles of green chemistry. Besides using renewable feedstock, safer solvents and auxiliaries (i.e. guaiacol and *n*-heptane), selective recyclable zeolite catalysis and waste prevention (recycling solvents by distillation), most importantly, chemical products were designed to preserve efficacy of function while reducing toxicity. The use of renewable feedstock was even taken a step further by direct implementation of a crude alkene-enriched lignin oil extract, obtained via a real wood biorefinery concept. This not only highlighted the robustness but also the industrial relevance of the proposed process to serve as a valuable downstream process in future lignocellulosic biorefinery schemes.

Methods

Chemicals and materials. For a list of all used chemicals and materials, the reader is kindly referred to **Supplementary M1**.

Reaction procedures. In a typical batch reaction, 20 mmol of guaiacol (2.534 g) and 1 mmol of 4-alkenylguaiacol (**1a-1e**) were added to 0.05 mmol catalytic H^+ (Supplementary M2) in a 10 mL round-bottom flask containing a magnetic stirring bar (13 x 3 mm). The flask was sealed with a rubber septum and flushed with N_2. To start the reaction, the flask was submerged in a pre-heated magnetically stirred (stir bar: 25 x 6 mm, 750 rpm) temperature-controlled oil bath for 2 hours at 80°C. Afterwards the reaction

was quenched in ice water and subsamples for GC-FID, HPLC-UV and GPC-PDA analysis were taken and filtered using a Millex®-FH hydrophobic PTFE Syringe Filter (0.45 µm pore size, 13 mm).

In a typical fed-batch reaction, 20 mmol of guaiacol (2.534 g) was added to 0.05 mmol catalytic H^+ (Supplementary M2) in a 10 mL round-bottom flask containing a magnetic stirring bar (13 x 3 mm). The flask was sealed with a rubber septum and flushed with N_2. The flask was submerged in a pre-heated magnetically stirred (stir bar: 25 x 6 mm, 750 rpm) temperature-controlled oil bath at 80°C. To start the reaction, the 4-alkenylguaiacol (**1a-b**) was continuously administered (flowrate: 1 mmol h^{-1}) *via* a syringe infusion pump system (B. Braun Perfusor® Space) equipped with a long needle (B. Braun Sterican®, 0.8 x 120 mm) and 20 mL syringe (BD Discardit™). After addition, the reaction was stirred for one extra hour to reach full conversion, and then quenched in ice water. To determine the exact amount of **1a-b** added, the flask was weighed before and after addition. Subsamples for GC-FID, HPLC-UV and GPC-PDA analysis were taken and filtered using a Millex®-FH hydrophobic PTFE Syringe Filter (0.45 µm pore size, 13 mm).

In a typical multi-gram scale reaction, the standard reaction procedure (in batch and/or fed-batch mode) was performed on larger scale to produce several grams of selected bisguaiacols (**2a-d**). Synthesis of up to 45 mmol of **2a** (≈ 13 g), 24 mmol of **2b** (≈ 6.5 g) and 6 mmol of **2c** (≈ 2 g) and **2d** (≈ 2 g) were performed. All parameters and equivalents were kept constant, except that the addition time of **1a** and **1b** was prolonged to 4 hours to assure high chemoselectivity.

In a typical kinetic experiment, 0.01 mmol catalytic H^+ (Supplementary M2) and 200 mmol of guaiacol (25.335 g, 22.78 mL) were added in a 25 mL round-bottom flask containing a magnetic stirring bar (13 x 3 mm). The flask was sealed with a rubber septum and flushed with N_2 before starting the reaction. The flask was submerged in a pre-heated (40–80°C) magnetically stirred (stir bar: 25 x 6 mm, 750 rpm) temperature-controlled oil bath. After 10 minutes the reaction was started by adding 1.25 mmol of **1a** (0.207 g). To monitor product formation, intermediate subsamples (200 mg) were taken for GC-FID analyses after 5, 10, 15, 20, 25, 30, 40, 50, 60, 90, 120 and 240 minutes of reaction and immediately quenched by (*i*) filtration using a Millex®-FH hydrophobic PTFE Syringe Filter, 0.45 µm pore size, 13 mm, and by (*ii*) addition of 200 µL pyridine and kept cold in ice water.

Reaction analysis – product characterization. GC-FID analysis was performed on an Agilent GC system (6890 series) with an Agilent HP5 capillary column (30 m x 0.32 mm, film thickness of 0.25 µm), equipped with an FID detector and ChemStation software. Prior to GC-FID analysis, the samples were derivatised *via* trimethylsilylation with MSTFA. In a typical sample preparation, 10 mg of internal standard (i.e. 4-propylguaiacol or 2-isopropylguaiacol), 200 µL of anhydrous pyridine, 500 µL of MSTFA, and 200 µL of acetonitrile were added to 200 mg (reaction mixture) or 5–10 mg (pure compounds) of sample. To guarantee complete derivatization, the vials were closed and heated for 20 min at 80 ^{o}C.

GC-MS analysis was performed on an Agilent GC system (6890 series) with a HP5 capillary column, equipped with an Agilent Mass Spectroscopy detector (5973 series) and used to identify unknown signals. Prior to GC-MS analysis, only **2c** was derivatized *via* trimethylsilylation with MSTFA.

Reversed-phase HPLC-UV systems were used (*i*) to confirm the quantitative analysis obtained by GC-FID and (ii) to fractionate and isolate bisguaiacol regioisomers and/or side-products. The quantitative analysis was performed on a Waters Alliance HPLC system (e2695 seperation module), equipped with a C_{18} –column (SUPELCOSIL™ LC-18, 250 mm x 4.6 mm, 5 µm) and a UV/Vis detector (2489 UV/Vis detector) at 280 nm. The fractionation of regioisomers and side-products was performed on a Shimadzu reversed-phase preparative HPLC system (Prominence system, system units specified in supplementary M3) equipped with a C_{18} column: (i) prep HPLC guard column (Shim-Pack GIS (G) C18 50 mm*20 mm, 5 µm) and (ii) prep HPLC column (Shim-Pack GIS C18 250 x 20mm, 5 µm), UV/Vis detector (SPD-20A) at 280 nm and fraction collector (FRC-10A).

GPC/SEC analysis was used for (i) qualitative analysis of the bisguaiacol reaction mixtures, detection of oligomers and (ii) to determine the MW distribution of the as-synthesized polymers. For the former a Waters Alliance GPC system (e2695 seperation module) was used, equipped with an Agilent PLgel column (Mixed E, 3 µm) and a Waters 2998 photodiode array (PDA) detector. For the latter, a Shimadzu SEC system was used, equipped with an Agilent PLgel column (Mixed-D, 300 x 7.5 mm, 5 µm) and UV/Vis detector (SDP-10Avp) at 254 nm. In general, to acquire and process the data obtained by liquid chromatography, Empower 3 software was used for the Waters HPLC/GPC systems and LabSolutions software was used for the Shimadzu HPLC/GPC systems.

The analytical methodology used for GC-FID, GC-MS, HPLC and GPC/SEC and quantification details are provided in Supplementary M3.

Liquid-phase ^{1}H, ^{13}C,^{13}C DEPT-135° and ^{1}H-^{13}C HSQC and HMBC nuclear magnetic resonance (NMR) spectra were acquired on Bruker Avance instruments (300 and 400 MHz) with automated samplers. In a typical sample preparation, 5–30 mg of dried sample was dissolved in 500 µL of deuterated solvent (i.e. $CDCl_3$, DMSO-d_6 and acetone-d_6).

TGA was used to determine the thermal stability of bisguaiacols and polymers. Using a TGA Q500 from TA Instruments equipped with autosampler, 10–20 mg of sample was heated under a N_2 atmosphere to 600°C at 10°C min^{-1}.

DSC was used to determine the T_m (bisguaiacols), the T_g (thermoplastics) and the degree of cure (thermoset) by using a DSC Q200 from TA Instruments. The temperature program consisted out of two heating-cooling cycles between (i) 20–160°C (bisguaiacols), (ii) 20–200°C (polycarbonates), (iii) 20–375°C (polyesters) at 10°C min^{-1} under a N_2 atmosphere, and (iv) 20–300°C (epoxy resins) at 10–20°C min^{-1} under N_2 atmosphere. Samples of 3–5 mg were precisely weighed in aluminum pans and covered with hermetic lids.

DMA was used to determine the T_g of the epoxy resins by using a DMA Q800 from TA Instruments with single cantilever clamp. The temperature program consisted of a heating ramp between 20–200°C at 2°C min^{-1} (20 µm amplitude, 1Hz frequency). T_g is defined as the max. tan (δ) temperature.

The data acquired by TGA, DSC and DMA analysis was processed with TA Universal Analysis.

Product work-up. After a multi-gram scale synthesis the reaction mixture was filtered and excess guaiacol was removed via reduced pressure distillation (90 ^{o}C, 7 mbar), yielding a product that mainly consisted of bisguaiacol regioisomers and a small amounts of cyclic dimers/oligomers. For **2a**, **2b** and **2d**, the *p,p'*-regioisomers were purified and isolated by hot (re)crystallization from *n*-heptane. The obtained crystals were dried *in vacuo*, pulverized and analyzed by GC-FID to assess the purity. Samples were recrystallized in case the regioisomeric purity was below 99.5%. The isolated yield of *p,p'*-regioisomer obtained by crystallization depends on (i) the presence of trace amounts guaiacol and/or cyclic dimers and (ii) product solubility and varies between 25–60 wt.%. For **2c**, the *p,p'*-regioisomer needed to be fractionated by preparative reversed-phase HPLC to obtain a highly pure (≥ 99.5%) compound.

- *4,4'-(propane-1,1-diyl)bis(2-methoxyphenol) – p,p'-*2a *– p,p'-BGP*

Off-white solid. m.p. (121°C). **^{1}H NMR** (400 MHz, $CDCl_3$, 25°C, TMS): δ_H (ppm) = 0.90 (t, *J* = 7.3 Hz, 3H), 2.00 (q, *J* = 7.4 Hz, 2H), 3.65 (t, *J* = 7.8 Hz, 1H); 3.86 (s, 6H), 5.51 (s, 2H), 6.69 (d, *J* = 2.0 Hz, 2H), 6.76 (dd, *J* = 8.1, 2.0 Hz, 2H), 6.85 (d, *J* = 8.1, 2H). **^{13}C NMR** (100 MHz, $CDCl_3$, 25°C, TMS): δ_C (ppm) = 12.9, 29.1, 52.5, 55.9, 110.6, 114.1, 120.2, 137.5, 143.8, 146.4. **MS** (70 eV, EI): m/z (%): 288 (18) [$M^{\bullet+}$], 259 (100) [$M^{\bullet+}$ + $^{\bullet}C_2H_5$].

- *4,4'-(ethane-1,1-diyl)bis(2-methoxyphenol) – p,p'-*2a *– p,p'-BGE*

White solid. m.p. (108°C). **^{1}H NMR** (400 MHz, $CDCl_3$, 25°C, TMS): δ_H (ppm) = 1.6 (d, *J* = 7.2 Hz, 3H), 3.83 (s, 6H), 4.02 (q, *J* = 7.2 Hz, 1H); 5.51 (s, 2H), 6.68 (d, *J* = 2.0 Hz, 2H), 6.75 (dd, *J* = 8.2, 2.0 Hz, 2H), 6.85 (d, *J* = 8.1, 2H). **^{13}C NMR** (100 MHz, $CDCl_3$, 25°C, TMS): δ_C (ppm) = 22.5, 44.1, 55.9, 110.4, 114.1, 120.0, 138.8, 143.8, 146.4. **MS** (70 eV, EI): m/z (%) = 274 (31) [$M^{\bullet+}$], 259 (100) [$M^{\bullet+}$ + $^{\bullet}CH_3$].

- *3,3'-bis(4-hydroxy-3-methoxyphenyl)propanoic acid – p,p'-*2c *– p,p'-BGPacid*

White solid. m.p. (69°C). **^{1}H NMR** (400 MHz, DMSO-d_6, 25°C, TMS): δ_H (ppm) = 2.91 (d, *J* = 8.0 Hz, 2H), 3.73 (s, 6H), 4.21 (t, *J* = 8.0 Hz, 1H); 6.66 (d, *J* = 8.1 Hz, 2H), 6.67 (dd, *J* = 8.0, 1.5 Hz, 2H), 6.85 (d, *J* = 1.6, 2H), 8.71 (s, 2H), 11.99 (s, 1H). **^{13}C NMR** (100 MHz, $CDCl_3$, 25°C, TMS): δ_C (ppm) = 41.0, 46.4, 56.1, 112.4, 115.7, 119.9, 136.1, 145.2, 147.8, 173.4. **MS** (70 eV, EI, trimethylsilylation): m/z (%) = 534 (18) [$M^{\bullet+}$], 403 (100) [$M^{\bullet+}$ + $^{\bullet}C_5H_{11}O_2Si$].

- *methyl 3,3'-bis(4-hydroxy-3-methoxyphenyl)propanoate – p,p'-*2d *– p,p'-BGPesterM*

White solid. m.p. (118°C). **^{1}H NMR** (400 MHz, $CDCl_3$, 25°C, TMS): δ_H (ppm) = 2.98 (d, *J* = 8.0 Hz, 2H), 3.59 (s, 3H), 3.82 (s, 6H), 4.42 (t, *J* = 8.0 Hz, 1H); 1.95 (s, 2H), 6.68 (d, *J* = 2.0 Hz, 2H), 6.73 (dd, *J* = 8.1, 2.0 Hz, 2H), 6.83 (d, *J* = 8.1, 2H). **^{13}C NMR** (100 MHz, $CDCl_3$, 25°C, TMS): δ_C (ppm) = 41.2, 46.3, 51.7, 55.8, 110.49,

114.3, 119.9, 135.7, 144.2, 146.5, 172.5. **MS** (70 eV, EI): m/z (%) = 332 (23) [$M^{\bullet+}$], 259 (100) [$M^{\bullet+}$ + $^{\bullet}C_3H_5O_2$].

In vitro **estrogen receptor transactivation bioassays.** The estrogenic activity of the bisphenols and bisguaiacols was determined in two *in vitro* human ERα transactivation bioassays, more particular the MELN and CALUX bioassays. In both assays, the hERα transcriptional activity is determined using human breast cancer MCF-7 cells that are stably transfected with an estrogen responsive luciferase gene plasmid which responds to estrogenically active compounds, resulting in the induction of luciferase reporter gene expression. The activity is measured in relative light units (RLU) and presented as induction of ER activation relative to luciferase induction of the positive control (17β-E2) (set at 100%).

Whereas the MELN assay uses MELN cells, defined as MCF-7 cells stably transfected with the estrogen-responsive gene ERE-βGlo-Luc-SVNeo, the CALUX assay uses VM7Luc4E2 cells, defined as MCF-7 cells stably transfected with the estrogen-responsive gene pGudLuc7.ERE. The MELN assay is performed as reported previously by Witters *et al.* (2010)[63] with slight modifications and the CALUX assay is performed as described by Vandermarken *et al.* (2016).[64] For a detailed description of the complete experimental procedure, the reader is kindly referred to Supplementary M5.

Results from three replicate cellular exposures, in three independent experiments (i.e. 3 x 3) for each test condition were averaged ± standard deviation (SD) using Graphpad Prism software (version 9.1.0, 2021) with calculation of EC_{50} by fitting a four-parameter sigmoidal dose-response curve (cf. Hill equation). To obtain EC_{50} values for partial concentration-response curves, the fit was constrained at the top and/or bottom value. However, if the fit seemed unreliable (i.e. R-squared < 0.95), no EC_{50} concentration was defined (N/A). The REE was determined as the top value of the induction relative to the positive control (17β-E2).

Polymerization. Polyesters were synthesized on a mg scale *via* interfacial polymerization with terephthaloyl chloride, according to methods reported previously with slight modifications.[23,65,66] In a two-neck round bottom flask (25 mL), under continuous stirring 1.7 mL of 1 M $NaOH_{aq}$ was added to 0.8 mmol of the bisphenol or bisguaiacol (> 99.5%) at 10°C. Once dissolved, 9.3 mg of benzyl triethyl ammonium chloride (BTEACl) was added, and the polymerization was initiated through the addition of a stoichiometric amount of terephthaloyl chloride (TPC) dissolved in DCM (4.6 mL) and the mixture was vigorously stirred for 1 hour at 10°C. After reaction, the reaction mixture was first precipitated in distilled water (150 mL, 50°C), filtrated, and washed with distilled water (3 x 50 mL), then dissolved in chloroform to precipitate it again in cold methanol, filtered and washed with methanol (3 x 50 mL). Finally, the polymer was dried *in vacuo* (80°C, ~ 1 mbar). Polymer yield is calculated from the theoretical molar mass of the repeating units, being 358.38 g mol^{-1} and 418.43 g mol^{-1} for **4a**-PT and **2a**-PT, respectively. Assuming that the total amount of end-groups is negligible to the total polymer weight.

Polycarbonates were prepared on a gram scale via interfacial polymerization with triphosgene, according the method reported previously by Koelewijn *et al.*[22,29] CAREFUL: SAFETY RULES AND PRECAUTIONS

THAT ARE AT LEAST AS STRICT AS THOSE FOR PHOSGENE MUST BE APPLIED. In a two-neck round bottom flask (25 mL), under continuous stirring 4 mL of 1.8 M $NaOH_{aq}$ was added to 2.2 mmol of the bisphenol or bisguaiacol (> 99.5%). Once dissolved, a solution of triphosgene (1.3 mmol, 0.375 g) in DCM (4 mL) was added and stirred for 30 min at 25°C. TEA (6 µL) and 50% (w/v) aqueous tetrabutylammonium chloride (3 µL) were added and the mixture was vigorously stirred for 5 h at 25°C. After reaction, the organic phase was separated and washed with distilled water (3 x 50 mL), neutralized with HCl, and precipitated in hot water (100 mL, 60°C). After filtration, the polymer was dried *in vacuo* (80°C, ~ 1 mbar).

The polymer yield was calculated from the theoretical molar mass of the repeating units, being 254.28, 314.33 g mol^{-1} for **4a**-PC and **2a**-PC, respectively, assuming that the total amount of end-groups is negligible to the total polymer weight.

Epoxy Resins were prepared in a two-step reaction process. In the first step, 4–12 mmol of **2a** and 0.2 eq. of the catalyst (TEBAC) were dissolved in an excess of 20 eq. epichlorohydrin in a sealed single-neck round-bottom flask. After purging with N_2 gas for 5 min, the reaction was started in a temperature-controlled oil bath (80°C) and stirred (750 rpm) for 3 h. Subsequently, the reaction mixture was cooled down in an ice batch (0°C). The second step was initiated by adding dropwise 4 eq. of NaOH in a 40 wt.% aqueous solution to the stirred reaction vessel at RT. After 3 hours of reaction, 110 mL of DCM was added and the reaction mixture was washed until pH 7 was reached. The organic phase was then dried over magnesium sulphate, filtered, and concentrated via reduced pressure distillation. Prior to analysis (^{1}H-NMR, HPLC and GPC), solvent trace amounts were removed *in vacuo* overnight. **2a**-DGE was obtained as an off-white solid m.p. 94°C with an absolute yield of 94% and purity higher than 97 mol%. The benchmark BPA (**4a**-DGE) epoxy resin was commercially purchased (BADGE). The epoxide equivalent weight (EEW) was determined by (^{1}H-NMR). To prepare rectangular cured epoxy resins (9 mm x 12 mm x 1 mm) for DMA, DSC and TGA analysis the epoxy resins were mixed, after melt and cool down, with stoichiometric amounts of isophorone diamine (IPDA) (i.e. stoichiometric amounts of mole diglycidyl ether groups to mole amine hydrogens) and air was removed *in vacuo*. Afterwards the mixture was poured into a silicone mold (Smooth-Sil® 950) and cured following the cure protocol: 1 h at 80°C, 1 h at 110°C and 1 h at 160°C.

RCF and monomer extraction. The RCF experiment was performed in a 100 mL stainless steel batch reactor (Parr Instruments & Co.). 4 g of the extracted substrate (250–500 µm) (Supplementary M6) was loaded into the reactor, together with 0.4 g of 5 wt.% Ru/C, 20 mL of *n*-butanol and 20 mL of water. Subsequently, the reactor was sealed, flushed three times with N_2 (5 bar) and then pressurized with H_2 (1 bar). After a reaction of 2 hours at 200°C, stirred at 750 rpm, the reactor was cooled and depressurized at RT. The reaction mixture was quantitatively collected using *n*-butanol and water and filtered to separate the solid residue (pulp and catalyst) from the liquid products. The solid pulp was washed with additional water and *n*-butanol, obtaining a biphasic filtrate. The two phases were separated, followed by two wash steps of the aqueous phase with fresh *n*-butanol to extract all depolymerized lignin. The butanol fractions

were collected, and *n*-butanol was evaporated by reduced pressure distillation yielding a viscous orange-brown lignin oil.

The following extraction steps were performed to increase the overall monomer concentration in the lignin oil. In general, the dry lignin oil is extracted at 80°C for 0.5 hours with 7 mL of solvent (95 vol.% *n*-heptane/5 vol.% ethyl acetate). One extraction step included three heating cycles and after each cycle the soluble fraction was collected. Subsequently, the solvent was removed via reduced pressure distillation to yield a crude lignin oil extract enriched in **1a**. In total, two extraction steps were performed to yield 160 mg of a yellow-orange crude lignin oil extract containing a monomer fraction of 51 wt.%.

References

1.Schnell, Hermann. Linear Aromatic Polyesters of Carbonic Acid. *Ind. Eng. Chem.* **51,** 157–160 (1959).

2.Pham, H. Q. in *Epoxy Resins, Ullmann's Encyclopedia of Industrial Chemistry* (Wiley-VCH, 2005).

3.Abts, G. & Wehrmann, R. in *Polycarbonates, Ullmann's Encyclopedia of Industrial Chemistry* (Wiley-VCH, 2014).

4.Fiege, H., Hamamoto, T., Umemura, S., Iwata, T., Miki, H., Fujita, Y., Buysch, H.-J., Garbe, D. & Paulus, W. in *Phenol derivatives, Ullmann's Encyclopedia of Industrial Chemistry* (Wiley-VCH, 2000).

5.Dodds, E. C. & Lawson, W. Synthetic Estrogenic Agents Whitout The Phenanthrene Nucleus. *Nature* **137,** 996 (1936).

6.Krishnan, A. V., Stathis, P., Permuth, S. F., Tokes, L. & Feldman, D. Bisphenol-A: an estrogenic substance is released from polycarbonate flasks during autoclaving. *Endocrinology* **132,** 2279–2286 (1993).

7.Brotons, J. A., Olea, -Serrano M. F., Villalobos, M., Pedraza, V. & Olea, N. Xenoestrogens released from lacquer coatings in food cans. *Environmental Health Perspectives* **103,** 608–612 (1995).

8.Olea, N., Pulgar, R., P, érez P., Olea, -Serrano F., Rivas, A., Novillo, -Fertrell A., Pedraza, V., Soto, A. M. & Sonnenschein, C. Estrogenicity of resin-based composites and sealants used in dentistry. *Environmental Health Perspectives* **104,** 298–305 (1996).

9.Corrales, J., Kristofco, L. A., Steele, W. B., Yates, B. S., Breed, C. S., Williams, E. S. & Brooks, B. W. Global Assessment of Bisphenol A in the Environment: Review and Analysis of Its Occurrence and Bioaccumulation. *Dose-Response* **13,** 1–29 (2015).

10.Howdeshell, K. L., Hotchkiss, A. K., Thayer, K. A., Vandenbergh, J. G. & vom Saal, F. S. Exposure to bisphenol A advances puberty. *Nature* **401,** 763–764 (1999).

11.Nadal, A. Fat from plastics? Linking bisphenol A exposure and obesity. *Nat Rev Endocrinol* **9,** 9–10 (2013).

12.Rochester, J. R. Bisphenol A and human health: A review of the literature. *Reproductive Toxicology* **42,** 132–155 (2013).

13.Heindel, J. J., Newbold, R. & Schug, T. T. Endocrine disruptors and obesity. *Nat Rev Endocrinol* **11,** 653–661 (2015).

14.Heindel, J. J., Belcher, S., Flaws, J. A., Prins, G. S., Ho, S.-M., Mao, J., Patisaul, H. B., Ricke, W., Rosenfeld, C. S., Soto, A. M., vom Saal, F. S. & Zoeller, R. T. Data integration, analysis, and interpretation of eight academic CLARITY-BPA studies. *Reprod. Toxicol.* **98,** 29–60 (2020).

15.Vom Saal, F. S. & Vandenberg, L. N. Update on the Health Effects of Bisphenol A: Overwhelming Evidence of Harm. *Endocrinology* **162,** bqaa171 (2021).

16.Eladak, S., Grisin, T., Moison, D., Guerquin, M.-J., N'Tumba-Byn, T., Pozzi-Gaudin, S., Benachi, A., Livera, G., Rouiller-Fabre, V. & Habert, R. A new chapter in the bisphenol A story: bisphenol S and bisphenol F are not safe alternatives to this compound. *Fertil. Steril.* **103,** 11–21 (2015).

17.Zimmerman, J. B. & Anastas, P. T. Toward substitution with no regrets. *Science* **347,** 1198–1199 (2015).

18.Moon, M. K. Concern about the Safety of Bisphenol A Substitutes. *Diabetes Metab J* **43,** 46–48 (2019).

19.Warner, G. R. & Flaws, J. A. Common bisphenol A replacements are reproductive toxicants. *Nat Rev Endocrinol* **14,** 691–692 (2018).

20.Liguori, F., Moreno-Marrodan, C. & Barbaro, P. Biomass-derived chemical substitutes for bisphenol A: recent advancements in catalytic synthesis. *Chem. Soc. Rev.* **49,** 6329–6363 (2020).

21.Soto, A. M., Schaeberle, C., Maier, M. S., Sonnenschein, C. & Maffini, M. V. Evidence of Absence: Estrogenicity Assessment of a New Food-Contact Coating and the Bisphenol Used in Its Synthesis. *Environ. Sci. Technol.* **51,** 1718–1726 (2017).

22.Koelewijn, S.-F., Van den Bosch, S., Renders, T., Schutyser, W., Lagrain, B., Smet, M., Thomas, J., Dehaen, W., Van Puyvelde, P., Witters, H. & Sels, B. F. Sustainable bisphenols from renewable softwood lignin feedstock for polycarbonates and cyanate ester resins. *Green Chem.* **19,** 2561–2570 (2017).

23.Koelewijn, S.-F., Cooreman, C., Renders, T., Andecochea Saiz, C., Van den Bosch, S., Schutyser, W., De Leger, W., Smet, M., Van Puyvelde, P., Witters, H., Van der Bruggen, B. & Sels, B. F. Promising bulk production of a potentially benign bisphenol A replacement from a hardwood lignin platform. *Green Chem.* **20,** 1050–1058 (2018).

24.Janvier, M., Hollande, L., Jaufurally, A. S., Pernes, M., Ménard, R., Grimaldi, M., Beaugrand, J., Balaguer, P., Ducrot, P.-H. & Allais, F. Syringaresinol: A Renewable and Safer Alternative to Bisphenol A for Epoxy-Amine Resins. *ChemSusChem* **10,** 738–746 (2017).

25.Trita, A. S., Over, L. C., Pollini, J., Baader, S., Riegsinger, S., Meier, M. a. R. & Gooßen, L. J. Synthesis of potential bisphenol A substitutes by isomerising metathesis of renewable raw materials. *Green Chem.* **19,** 3051–3060 (2017).

26.Peng, Y., Nicastro, K. H., Epps, T. H. & Wu, C. Evaluation of Estrogenic Activity of Novel Bisphenol A Alternatives, Four Bioinspired Bisguaiacol F Specimens, by in Vitro Assays. *J. Agric. Food Chem.* **66,** 11775–11783 (2018).

27.Szafran, A. T., Stossi, F., Mancini, M. G., Walker, C. L. & Mancini, M. A. Characterizing properties of non-estrogenic substituted bisphenol analogs using high throughput microscopy and image analysis. *PLoS ONE* **12,** e0180141 (2017).

28.Peng, Y., Nicastro, K. H., Epps, III, T. H. & Wu, C. Methoxy groups reduced the estrogenic activity of lignin-derivable replacements relative to bisphenol A and bisphenol F as studied through two in vitro assays. *Food Chem.* **338,** 127656 (2021).

29.Koelewijn, S.-F., Ruijten, D., Trullemans, L., Renders, T., Van Puyvelde, P., Witters, H. & Sels, B. F. Regioselective synthesis, isomerisation, *in vitro* oestrogenic activity, and copolymerisation of bisguaiacol F (BGF) isomers. *Green Chem.* **21,** 6622–6633 (2019).

30.Amitrano, A., S. Mahajan, J., J. Korley, L. T. & H. Epps, T. Estrogenic activity of lignin-derivable alternatives to bisphenol A assessed via molecular docking simulations. *RSC Adv.* **11,** 22149–22158 (2021).

31.Vanholme, R., Demedts, B., Morreel, K., Ralph, J. & Boerjan, W. Lignin Biosynthesis and Structure. *Plant Physiol.* **153,** 895–905 (2010).

32.Zakzeski, J., Bruijnincx, P. C. A., Jongerius, A. L. & Weckhuysen, B. M. The Catalytic Valorization of Lignin for the Production of Renewable Chemicals. *Chem. Rev.* **110,** 3552–3599 (2010).

33.Ragauskas, A. J., Beckham, G. T., Biddy, M. J., Chandra, R., Chen, F., Davis, M. F., Davison, B. H., Dixon, R. A., Gilna, P., Keller, M., Langan, P., Naskar, A. K., Saddler, J. N., Tschaplinski, T. J., Tuskan, G. A. & Wyman, C. E. Lignin Valorization: Improving Lignin Processing in the Biorefinery. *Science* **344,** (2014).

34.Rinaldi, R., Jastrzebski, R., Clough, M. T., Ralph, J., Kennema, M., Bruijnincx, P. C. A. & Weckhuysen, B. M. Paving the Way for Lignin Valorisation: Recent Advances in Bioengineering, Biorefining and Catalysis. *Angew. Chem. Int. Ed.* **55,** 8164–8215 (2016).

35.Schutyser, W., Renders, T., Bosch, S. V. den, Koelewijn, S.-F., T. Beckham, G. & F. Sels, B. Chemicals from lignin: an interplay of lignocellulose fractionation, depolymerisation, and upgrading. *Chem. Soc. Rev.* **47,** 852–908 (2018).

36.Sun, Z., Fridrich, B., de Santi, A., Elangovan, S. & Barta, K. Bright Side of Lignin Depolymerization: Toward New Platform Chemicals. *Chem. Rev.* **118,** 614–678 (2018).

37.Renders, T., Bosch, S. V. den, Koelewijn, S.-F., Schutyser, W. & F. Sels, B. Lignin-first biomass fractionation: the advent of active stabilisation strategies. *Energy Environ. Sci.* **10,** 1551–1557 (2017).

38.Meier, D., Berns, J., Grünwald, C. & Faix, O. Analytical pyrolysis and semicontinuous catalytic hydropyrolysis of Organocell lignin. *Journal of Analytical and Applied Pyrolysis* **25,** 335–347 (1993).

39.A. Onwudili, J. & T. Williams, P. Catalytic depolymerization of alkali lignin in subcritical water: influence of formic acid and Pd/C catalyst on the yields of liquid monomeric aromatic products. *Green Chem.* **16,** 4740–4748 (2014).

40.Luo, H., Klein, I. M., Jiang, Y., Zhu, H., Liu, B., Kenttämaa, H. I. & Abu-Omar, M. M. Total Utilization of Miscanthus Biomass, Lignin and Carbohydrates, Using Earth Abundant Nickel Catalyst. *ACS Sus. Chem. Eng.* **4,** 2316–2322 (2016).

41.Anderson, E. M., Katahira, R., Reed, M., Resch, M. G., Karp, E. M., Beckham, G. T. & Román-Leshkov, Y. Reductive Catalytic Fractionation of Corn Stover Lignin. *ACS Sus. Chem. Eng.* **4,** 6940–6950 (2016).

42.Zhao, Z. & Moghadasian, M. H. Chemistry, natural sources, dietary intake and pharmacokinetic properties of ferulic acid: A review. *Food Chem.* **109,** 691–702 (2008).

43.Chandra, G., Nesakumar, E. J., Bhotla, V. R. G., Shetty, S. G., Mahood, J., Gallucci, R. R., Kamps, J. H. & Kumar, M. S. Alkoxy polycarbonates, bisphenol monomers and methods of making and using the same. US9120893. (2015).

44.Trullemans, L., Koelewijn, S.-F., Scodeller, I., Hendrickx, T., Van Puyvelde, P. & Sels, B. F. A guide towards safe, functional and renewable BPA alternatives by rational molecular design: structure–property and structure–toxicity relationships. *Polym. Chem.* **12,** 5870–5901 (2021).

45.Hernandez, E. D., Bassett, A. W., Sadler, J. M., La Scala, J. J. & Stanzione, J. F. Synthesis and Characterization of Bio-based Epoxy Resins Derived from Vanillyl Alcohol. *ACS Sustain. Chem. Eng.* **4,** 4328–4339 (2016).

46.Hambleton, K. M. & Stanzione, J. F. Synthesis and Characterization of a Low-Molecular-Weight Novolac Epoxy Derived from Lignin-Inspired Phenolics. *ACS Omega* **6,** 23855–23861 (2021).

47.Farnham, A. G. & Klosek, F. P. Manufacture of diphenylol methanes. US2812364A. (1957).

48.Cavani, F., Corrado, M. & Mezzogori, R. A note on the role of methanol in the homogeneous and heterogeneous acid-catalyzed hydroxymethylation of guaiacol with aqueous solutions of formaldehyde. *J. Mol. Cata. A Chem.* **182–183,** 447–453 (2002).

49.De Vos, D. E. & Jacobs, P. A. Zeolite effects in liquid phase organic transformations. *Micropor. Mesopor. Mat.* **82,** 293–304 (2005).

50.Galkin, M. V. & Samec, J. S. M. Selective Route to 2-Propenyl Aryls Directly from Wood by a Tandem Organosolv and Palladium-Catalysed Transfer Hydrogenolysis. *ChemSusChem* **7,** 2154–2158 (2014).

51.Xiao, L.-P., Wang, S., Li, H., Li, Z., Shi, Z.-J., Xiao, L., Sun, R.-C., Fang, Y. & Song, G. Catalytic Hydrogenolysis of Lignins into Phenolic Compounds over Carbon Nanotube Supported Molybdenum Oxide. *ACS Catal.* **7,** 7535–7542 (2017).

52.Martínez, C. & Corma, A. Inorganic molecular sieves: Preparation, modification and industrial application in catalytic processes. *Coord. Chem. Rev.* **255,** 1558–1580 (2011).

53.Grommet, A. B., Feller, M. & Klajn, R. Chemical reactivity under nanoconfinement. *Nat. Nanotechnol.* **15,** 256–271 (2020).

54.Åqvist, J., Kazemi, M., Isaksen, G. V. & Brandsdal, B. O. Entropy and Enzyme Catalysis. *Acc. Chem. Res.* **50,** 199–207 (2017).

55.Cooreman, E., Vangeel, T., Van Aelst, K., Van Aelst, J., Lauwaert, J., Thybaut, J. W., Van den Bosch, S. & Sels, B. F. Perspective on Overcoming Scale-Up Hurdles for the Reductive Catalytic Fractionation of Lignocellulose Biomass. *Ind. Eng. Chem. Res.* **59,** 17035–17045 (2020).

56.Kricheldorf, H. R. & Schwarz, G. Cyclic Polymers by Kinetically Controlled Step-Growth Polymerization. *Macromol. Rapid Commun.* **24,** 359–381 (2003).

57.Jang, B. N. & Wilkie, C. A. A TGA/FTIR and mass spectral study on the thermal degradation of bisphenol A polycarbonate. *Polym. Degrad. Stabil.* **86,** 419–430 (2004).

58.Cowie, J. M. G. & Arrighi, V. *Polymers: Chemistry and Physics of Modern Materials.* (CRC Press, Taylor & Francis group, 2007).

59.Dong, Q., Gao, C., Ding, Y., Wang, F., Wen, B., Zhang, S., Wang, T. & Yang, M. A polycarbonate/magnesium oxide nanocomposite with high flame retardancy. *J. Appl. Polym. Sci.* **123,** 1085–1093 (2012).

60.Gioia, C., Vannini, M., Celli, A., Colonna, M. & Minesso, A. Chemical recycling of post-consumer compact discs towards novel polymers for powder coating applications. *RSC Adv.* **6,** 31462–31469 (2016).

61.Liu, P., Zeng, L., Ye, G. & Xu, J. Bisphenol A-based co-polyarylates: synthesis, properties and thermal decomposition mechanism. *J Polym Res* **20,** 279 (2013).

62.Curia, S., Biundo, A., Fischer, I., Braunschmid, V., Gübitz, G. M. & Stanzione, J. F. Towards Sustainable High-Performance Thermoplastics: Synthesis, Characterization, and Enzymatic Hydrolysis of Bisguaiacol-Based Polyesters. *ChemSusChem* **11,** 2529–2539 (2018).

63.Witters, H., Freyberger, A., Smits, K., Vangenechten, C., Lofink, W., Weimer, M., Bremer, S., Ahr, P. H.-J. & Berckmans, P. The assessment of estrogenic or anti-estrogenic activity of chemicals by the human stably transfected estrogen sensitive MELN cell line: Results of test performance and transferability. *Reprod. Toxicol.* **30,** 60–72 (2010).

64.Vandermarken, T., De Galan, S., Croes, K., Van Langenhove, K., Vercammen, J., Sanctorum, H., Denison, M. S., Goeyens, L., Elskens, M. & Baeyens, W. Characterisation and implementation of the ERE-CALUX bioassay on indoor dust samples of kindergartens to assess estrogenic potencies. *J. Steroid Biochem. Mol. Biol.* **155,** 182–189 (2016).

65.Kuhire, S. S., Nagane, S. S. & Wadgaonkar, P. P. Pendant furyl containing bisphenols, polymers therefrom and a process for the preparation thereof. WO2015140818A4. (2015).

66.Ping, Z., Linbo, W. & Bo-Geng, L. Thermal stability of aromatic polyesters prepared from diphenolic acid and its esters. *Polym. Degrad. Stab.* **94,** 1261–1266 (2009).

Declarations

Data Availability.

The data available within the article and the supplementary information support all reported findings in this paper.

Acknowledgments

B.F.S thanks the KU Leuven industrial research fund (L.T. and S.F.K.), the financial support of Flanders Innovation & Entrepreneurship cluster Catalisti, cSBO Moonshot project (T.H., G.P. and H.W.) and the EOS project BIOFACT (E.C.). We greatly thank H.W. of the Flemish Institute for Technological Research (VITO) and I.M., M.E. of the Vrije Universiteit Brussel (VUB) for the *in vitro* estrogenic activity screenings, P.V.P. for the analyses of the thermal properties, and the KU Leuven biorefinery innovation manager (J.V.A.) and M.D for the interesting discussions. Patent applications are pending for inventors S.-F.K. and B.F.S. (EP/WO).

Author contributions

S.-F.K., L.T. and B.F.S. conceived and directed the project. S.-F.K. and L.T. carried out key experiments and wrote the manuscript. G.P. synthesized the polycarbonates. I.B. and M.E. performed the CALUX bioassay. T.H. and H.W. performed the MELN bioassay. E.C. and J.V.A. carried out the adapted RCF experiments. P.V.P. contributed to the screening of thermal properties and M.D. to the kinetic experimental design. All authors discussed the results and commented on the manuscript.

Competing interests

The authors declare no competing interests.

Figures

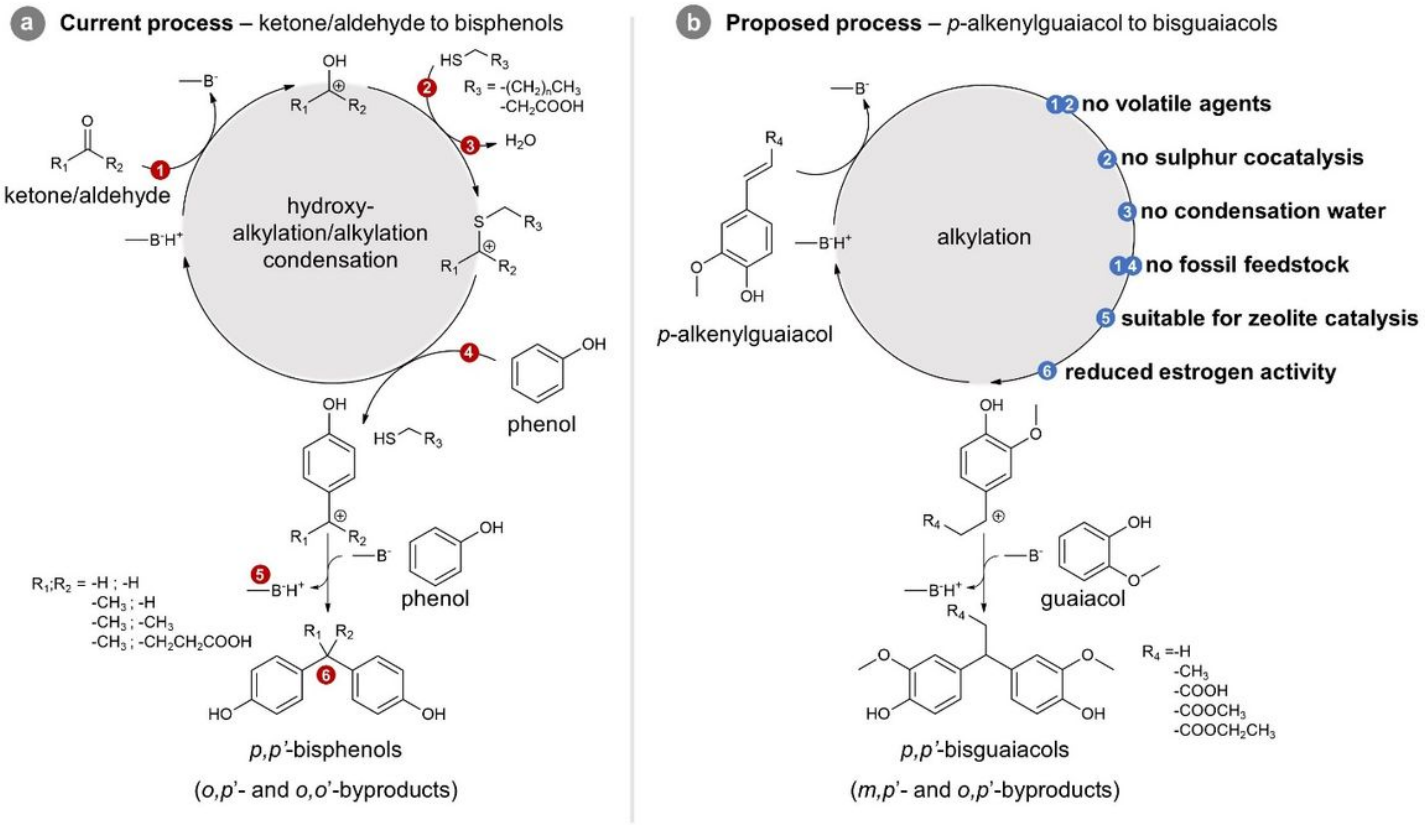

Figure 1

The sustainable advantages of the proposed bisguaiacol process *versus* current industrial bisphenol process. (**a**) The current industrial process produces xeno-estrogenic bisphenols from fossil ketone/aldehyde and phenol via hydroxyalkylation-alkylation condensation. Colored red dots indicate the unsustainable disadvantages of the process. Chemical structures of the most common ketone/aldehyde (R_1 and R_2), bisphenols (R_1 and R_2) and thiol co-catalyst (R_3) are given. (**b**) The proposed innovative process to obtain safer bisguaiacols from renewable lignin-derived *p*-alkenylguaiacol and guaiacol via Friedel-Crafts alkylation. Colored blue dots indicate the sustainable advantages of the proposed process compared to the industrial process. Chemical structures of the newly proposed *p*-alkenylguaiacols (R_4) and bisguaiacols (R_4) are given.

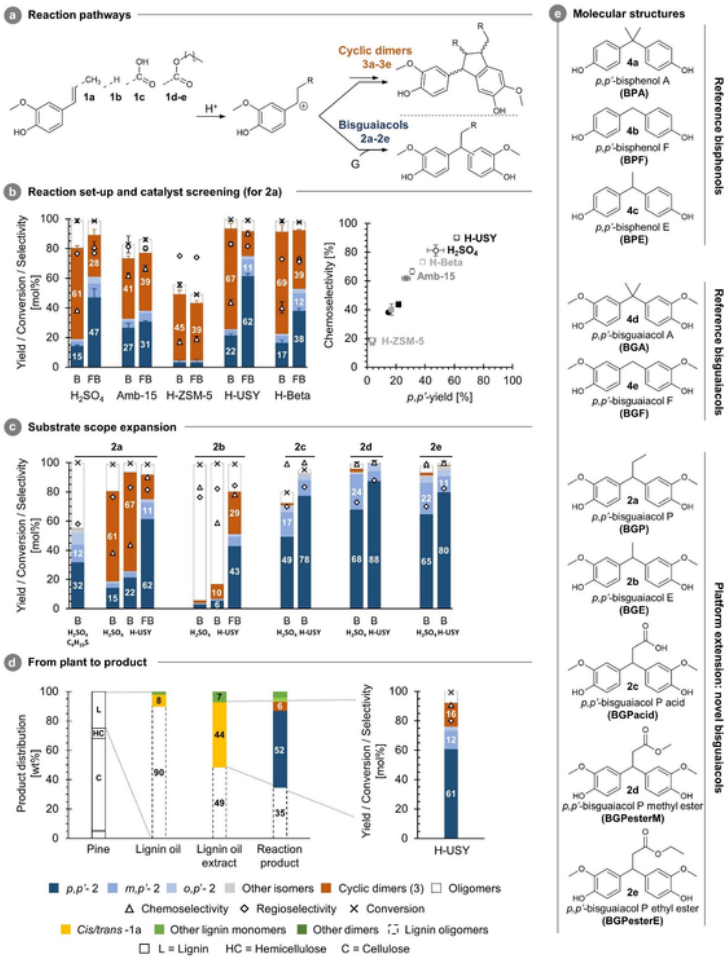

Fig. 2 | Product distributions. (**a**) Reaction pathways of *p*-alkenylguaiacols (**1**) into bisguaiacols (**2**, in blue) or cyclic dimers (**3**, in orange). (**b, left**) Yield, conversion, and selectivity (mol%) upon alkylating guaiacol (G) with **1a** for selected homo- and heterogeneous catalysts in batch (B, open symbols) and/or fed-batch (FB, closed symbols, at 1 mmol h^{-1}) reactor set-up. (**b, right**) Reaction systems (in terms of catalyst and/or set-up) are visualized by plotting chemoselectivity against *p,p'*-yield. (**c**) Yield, conversion, and selectivity (mol%) upon alkylating G with **1a-e** catalyzed by H_2SO_4 and zeolite H-USY. The hydroxyalkylation-alkylation condensation of G with propanal to **2a** (co-)catalyzed by H_2SO_4 and *n*-butanethiol (100 °C, 20 h) is shown as a benchmark. (**d, left**) Product distributions (in wt.%) in going from pine softwood (L: lignin, HC: hemicellulose, C: cellulose, blank: others) via lignin oil over crude lignin oil extract to alkylation reaction product. (**d, right**) Yield, conversion and selectivity (mol%) upon alkylating G with crude lignin oil extract (160 mg, 0.43 mmol **1a**) catalyzed by zeolite H-USY in high dilution B mode (130 mmol G). (**e**) Chemical structures of discussed bisphenols/bisguaiacols including numbering and abbreviations based on previously reported nomenclature[44]. Reaction conditions: 20 mmol of G, 1 mmol of **1a-e**, 0.05 mmol H^+, 80 °C, 2 h and 750 rpm. Note that **1a-b** are liquids and **1c-e** are solids at RT. Selected catalysts: sulfuric acid (H_2SO_4), Amberlyst 15 (Amb-15), H-ZSM-5 (Si/Al = 15), H-USY (CBV-780, Si/Al = 40), H-Beta (BEA-150, Si/Al = 75). Product quantification: GC-FID after trimethylsilylation. Definitions: yield (mol%): $\frac{product\ [mol]}{theoretical\ max.\ product\ [mol]} \times 100$, chemoselectivity (mol%): $\frac{2\ [mol]}{2\ [mol] + 3\ [mol]} \times 100$ and regioselectivity (mol%): $\frac{p,p'-2\ [mol]}{all\ regioisomers\ 2\ [mol]} \times 100$.

Figure 2

See figure for legend.

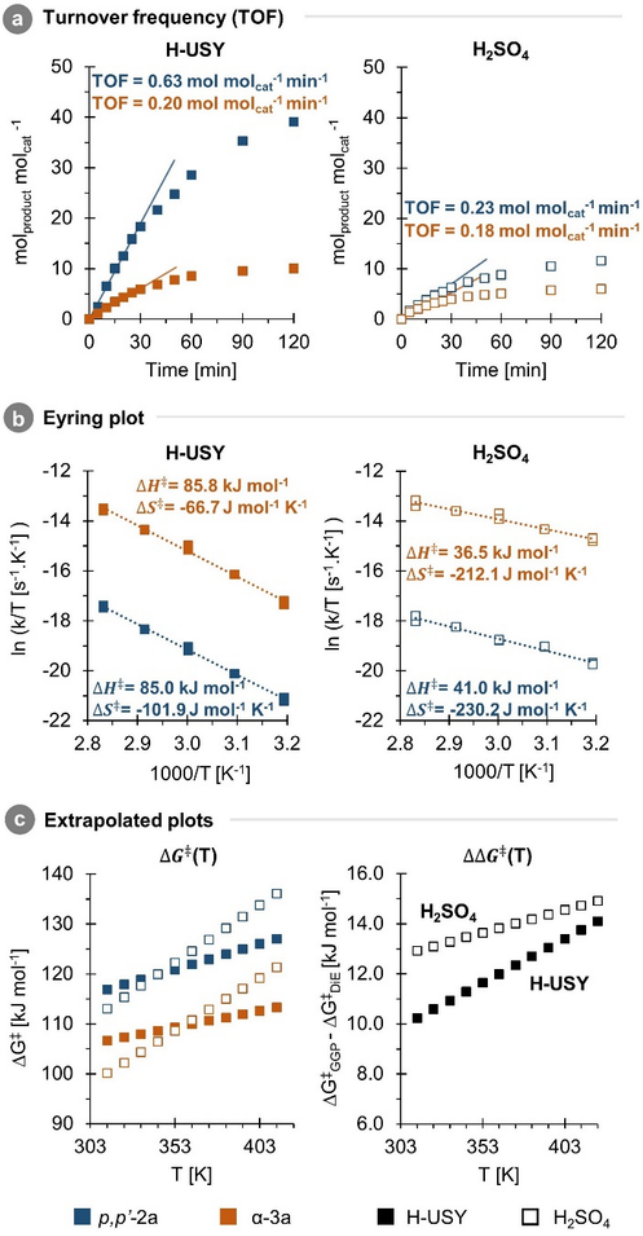

Fig. 3 | Kinetic analyses of *p,p'*-2a (in blue) and α-3a (in orange) formation by confined H-USY (closed) and unconfined H_2SO_4 (open) catalysis. (**a**) Catalytic efficiency (in $mol_{product} \cdot mol_{cat}^{-1}$) against time at 80 °C with indication of the corresponding (initial) turnover frequency (TOF). (**b**) Eyring plots with the corresponding $\Delta H^{\ddagger}$ and $\Delta S^{\ddagger}$ values. (**c**) $\Delta G^{\ddagger}$ and $\Delta(\Delta G^{\ddagger})$ as a function of (extrapolated) temperature for 313 to 413 K (40-140 °C). Reaction conditions: 1.25 mmol **1a**, 200 mmol G, 0.01 mmol H^+, 40-80 °C and 750 rpm.

Figure 3

See figure for legend.

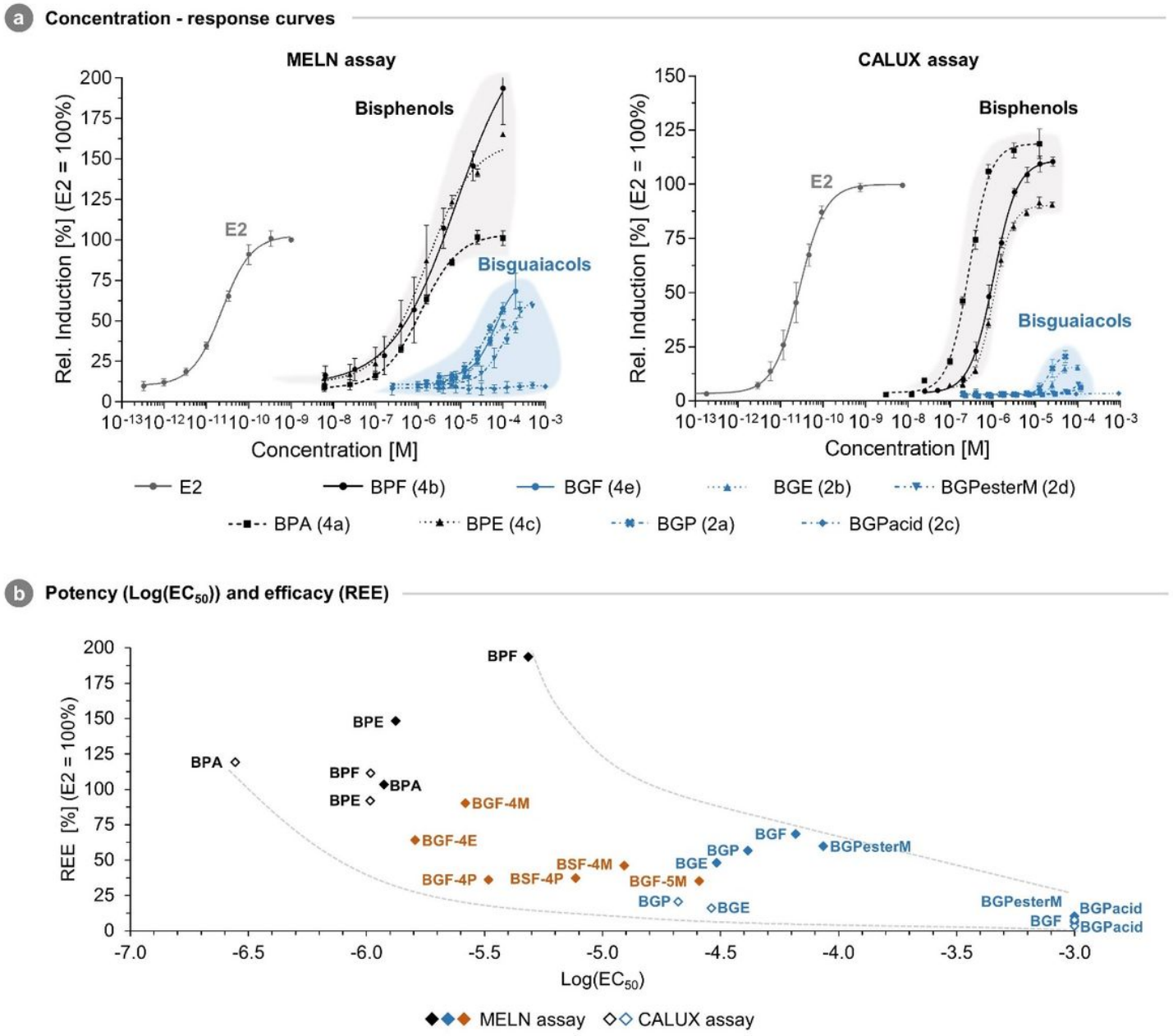

Figure 4

In vitro **human estrogen receptor α (hERα) activity of *p,p'*-bisguaiacols (in blue) and *p,p'*-bisphenols (in black).** (**a**) Concentration-response curves for (**left**) MELN and (**right**) CALUX bioassays. (**b**) Scatter plot of potency and efficacy expressed in terms of relative estrogenic efficacy (REE) and log-transformed half-maximal effective concentration ($log(EC_{50})$), respectively, as calculated for the MELN (closed diamonds) and/or CALUX (open diamonds) bioassay. Distinct clusters of responsiveness can be discerned grouping either *p,p'*-bisphenols (**4a-c**, in black), *p,p'*-bisguaiacols (**4e** and **2a-d**, in blue) or previously reported *m,m'*-bisguaiacols/-bissyringols (in orange).[22,23] Abbreviations as denoted in Figure 2 and ref. [22] and [23].

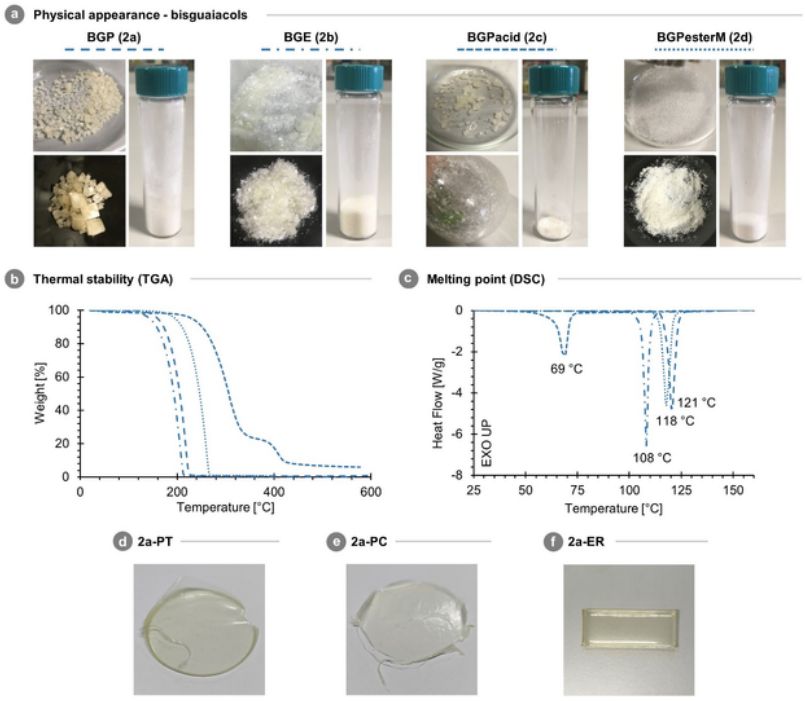

g Polymer properties

Thermoplastics	Yield	Physical properties								Thermal stability				
		Phase	Color	$\overline{M}_w$	$\overline{M}_n$	Đ	Crystalline	T_m	T_g	$T_{d,5\%}$	$T_{d,10\%}$	$T_{d,50\%}$	$T_{d,max}$	$Char_{600\,°C}$
	[%]			[kg mol^{-1}]	[kg mol^{-1}]			[°C]	[°C]	[°C]	[°C]	[°C]	[°C]	[%]
2a-PT	96	solid	off-white	132.0	31.9	4.1	no	-	166	373	396	473	425	29
4a-PT	95	solid	white	21.4	4.7	4.6	no	-	226	455	474	521	506	33
2a-PC	87	solid	yellowish	62.1	8.9	7.0	no	-	101	193	367	437	444	13
4a-PC	90	solid	white	25.3	3.5	7.3	no	-	118	337	446	519	521	23

Thermosets	Yield	Conversion degree	Physical properties						Thermal stability				
			Phase	Color	EEW	n	T_m	T_g	$T_{d,5\%}$	$T_{d,10\%}$	$T_{d,50\%}$	$T_{d,max}$	$Char_{600\,°C}$
	[%]	[%]			[g mol^{-1}]		[°C]	[°C]	[°C]	[°C]	[°C]	[°C]	[%]
2a-DGE	94	-	solid	off-white	204	0.02	94	-	216	236	283	298	0
4a-DGE	-	-	solid	white	173	0.02	46	-	234	250	294	312	0
2a-ER	-	93	solid	transparent	-	-	-	117	335	344	365	363	9
4a-ER	-	93	solid	transparent	-	-	-	173	346	355	377	366	8

Fig. 5 | Key physical and thermal properties of bisguaiacol monomers and polymers. (**a**) Physical appearances, (**b**) thermal stabilities (T_d) as measured by TGA under N_2, and (**c**) base-line corrected melting points (T_m) as determined (in the first heating cycle) by DSC under N_2 (at 10 °C min^{-1}) of the pure crystalline *p,p'*-bisguaiacols. Physical appearances of the *p,p'*-**2a**-based thermoplastic (**d**) polyterephthalate (**2a**-PT) and (**e**) polycarbonate (**2a**-PC), and thermosetting (**f**) epoxy resin (**2a**-ER) after curing with IPDA. (**g**) Thermophysical properties of the thermoplastics (**2a**-PT, **2a**-PC and **4a**-based benchmarks), uncured diglycidyl ethers (i.e. **2a**-DGE and **4a**-DGE) and IPDA-cured thermosetting epoxy resins (i.e. **2a**-ER and **4a**-ER). $\overline{M}_w$ and Đ derived by SEC in THF; epoxy equivalent weight (EEW) and degree of polymerization (*n*) derived by ^{1}H-NMR. T_m and T_g (thermoplastics) by DSC, T_g (thermosets) by DMA and the temperature at weight loss 5% ($T_{d,5\%}$), 10% ($T_{d,10\%}$), 50% ($T_{d,50\%}$), the maximal degradation ($T_{d,max}$) and char yield at 600 °C measured by TGA under N_2.

Figure 5

See figure for legend.

Supplementary Files

This is a list of supplementary files associated with this preprint. Click to download.

- 2022TrullemansL.KoelewijnS.F.etal.SupplementaryInformation.docx